EPJ Web of Conferences **127**, 00006 (2016) DOI: 10.1051/epjconf/201612700006
Connecting The Dots 2016

Machine Learning and Parallelism in the Reconstruction of LHCb and its Upgrade

Michel **De Cian**[1,a] on behalf of the LHCb collaboration

[1] *Physikalisches Institut der Universität Heidelberg, Germany*

Abstract. The LHCb detector at the LHC is a general purpose detector in the forward region with a focus on reconstructing decays of c- and b-hadrons. For Run II of the LHC, a new trigger strategy with a real-time reconstruction, alignment and calibration was employed. This was made possible by implementing an offline-like track reconstruction in the high level trigger. However, the ever increasing need for a higher throughput and the move to parallelism in the CPU architectures in the last years necessitated the use of vectorization techniques to achieve the desired speed and a more extensive use of machine learning to veto bad events early on. This document discusses selected improvements in computationally expensive parts of the track reconstruction, like the Kalman filter, as well as an improved approach to get rid of fake tracks using fast machine learning techniques. In the last part, a short overview of the track reconstruction challenges for the upgrade of LHCb, is given. Running a fully software-based trigger, a large gain in speed in the reconstruction has to be achieved to cope with the 40 MHz bunch-crossing rate. Two possible approaches for techniques exploiting massive parallelization are discussed.

1 Introduction

For Run II of the LHC, LHCb adopted a new trigger strategy with a real-time reconstruction, alignment and calibration. This allows to directly use the output of the trigger reconstruction to perform physics analyses [1]. To achieve this goal, the track reconstruction in the high-level software trigger (HLT, online) and offline had to be unified, to already obtain the best performance for the real-time alignment and calibration online. Several strategies were employed. A new sequence for the track reconstruction was implemented, which lead to a large speed up. This will be discussed in Section 2. For very computing intensive parts of the code, parallelization in the form of SIMD (single instruction, multiple data) instructions were used that lead to a large gain in time, see Section 3. Furthermore, machine learning methods were employed to reject tracks which do not originate from a real particle (Section 4). Section 5 then discusses the total gain in timing.

The upgraded LHCb detector, which will start taking data in 2020, will use a fully software-based trigger to cope with the 40 MHz bunch crossing rate. In Section 6 two possible strategies and one technical aspect on how to perform track reconstruction in this high multiplicity environment are discussed.

[a] e-mail: michel.de.cian@cern.ch

2 The LHCb detector

The LHCb experiment (see Figure 1) is dedicated to the study of beauty and charm hadron decays with special attention paid to CP violating phenomena as well as searches for physics beyond the Standard Model through rare decays. Since the beauty production cross-section is dominated by gluon fusion, which occurs in the forward region, the LHCb detector is a single-arm forward spectrometer with a pseudorapidity η spanning the range $1.8 < \eta < 4.9$ [2, 3]. The detector includes a high-precision tracking system consisting of a silicon-strip vertex detector (VELO) surrounding the pp interaction region, a large-area silicon-strip detector (TT) located upstream of a dipole magnet with a bending power of about 4 Tm, and three stations of silicon-strip detectors (IT) and straw drift tubes (OT) placed downstream of the magnet. The tracking system provides a measurement of the momentum p of charged particles with a relative uncertainty that varies from 0.5% at low momentum to 1.0% at 200 GeV/c. The minimum distance of a track to a proton-proton collision, the impact parameter, is measured with a resolution of $(15 + 29/p_{\mathrm{T}})$ µm, where p_{T} is the component of the momentum transverse to the beam, in GeV/c. Different types of charged hadrons are distinguished using information from two ring-imaging Cherenkov detectors (RICH1, RICH2). Photons, electrons and hadrons are identified by a calorimeter system consisting of scintillating-pad (SPD) and preshower detectors (PS), an electromagnetic calorimeter (ECAL) and a hadronic calorimeter (HCAL). Muons are identified by a system composed of alternating layers of iron and multi-wire proportional chambers (MUON).

The LHCb coordinate system is a right handed Cartesian system with the origin at the interaction point. The x-axis is oriented horizontally towards the outside of the LHC ring, the y-axis is pointing upwards with respect to the beam line and the z-axis is aligned with the beam direction.

The online event selection is performed by the trigger, which is composed of three stages: a stage implemented in hardware known as Level 0 (L0) and two stages implemented in software called High-Level-Trigger (HLT1 and HLT2). The HLT1 performs a partial reconstruction of the candidates. In this stage all requirements are inclusive, which means that the selection is applied only to subset of the final state particles. The HLT2 contains both inclusive and exclusive algorithms which are more time-consuming but provide a more precise reconstruction. Exclusive algorithms are used to select a specific decay at the trigger stage.

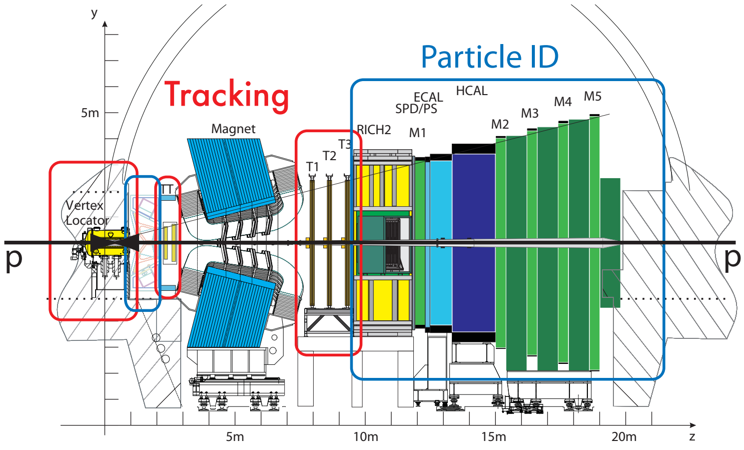

Figure 1. The LHCb detector at the LHC, with the tracking detectors (VELO, TT, T-stations) in red and the detectors for particle identification (RICH1, RICH2, calorimeters and muon system) in blue.

2.1 Track types

With its three tracking detectors, several track types can be reconstructed in LHCb, see Figure 2. The most important category are so-called long tracks, which traverse the full tracking systems and therefore deposit charge in the VELO, the T-stations and potentially also in TT. They are formed from daughters of promptly decaying particles and from daughters of b- and c-hadrons, which only travel a couple of mm before their decay. The other important type are so-called downstream tracks. They originate from daughters of long-living particles, which decay after the VELO and therefore are only reconstructed in TT and the T-stations. Long tracks are reconstructed using two dedicated algorithms. The first, called forward tracking, starts with VELO [4] or upstream tracks [5] and tries to find corresponding clusters in the T-stations [6]. The second, called track matching, uses tracks in the VELO and the T-stations [7] (called T tracks) as starting point and tries to match them in the magnet region [8, 9]. Downstream tracks are reconstructed by using tracks in the T-stations as starting point and extrapolating them back through the magnet [10].

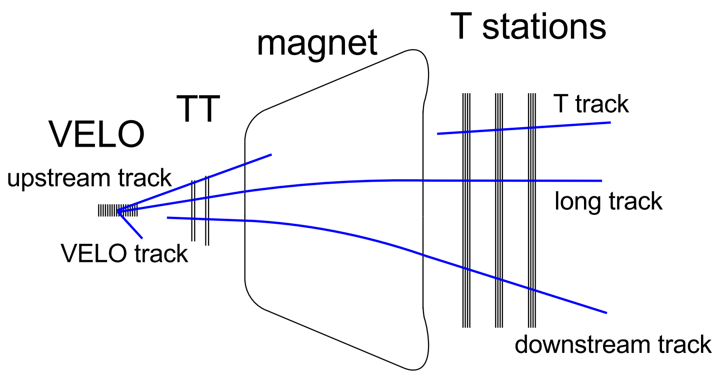

Figure 2. Track types in LHCb. Long tracks and downstream tracks are used for physics analyses, the other types either serve as a component of another track type or are used for detector studies.

2.2 Run II track reconstruction sequence

The run II track reconstruction sequence is split in an HLT1 and HLT2 part (see left part of Figure 3). In HLT1, all VELO tracks are reconstructed. These VELO tracks are fitted with a simplified Kalman filter (allowing for a single scattering at the sensor planes) and are then used to find the primary vertices. The VELO tracks are also extrapolated to TT, where clusters around the extrapolation are searched for. Due to the fringe field of the magnet this provides a first estimate of the sign of the charge. The tracks are then propagated through the magnet to the T-stations, searching for corresponding clusters, such that all tracks with a transverse momentum larger than 500 MeV/c are found (right part of Figure 3). The tracks found are fitted with a Kalman Filter.

Requiring clusters in TT when starting from VELO tracks significantly reduces the time spent in HLT1 to find long tracks, as tracks with low momenta will not have corresponding clusters in TT and therefore will not be propagated through the magnet. Furthermore, having a charge estimate reduces the search window for clusters in the T-stations by a factor of two. And finally, VELO tracks which are fakes will not get confirmed if no clusters in TT are found.

In HLT2, the HLT1 reconstruction part is repeated first. Then all VELO tracks which could not be made into long tracks are again propagated to the T-stations, however without requiring clusters in TT or a cut on the transverse momentum. In addition, T tracks are reconstructed and combined with VELO tracks, to form long tracks, and with clusters in TT, to form downstream tracks. All tracks are fitted with a Kalman filter and clones from the different algorithms are removed.

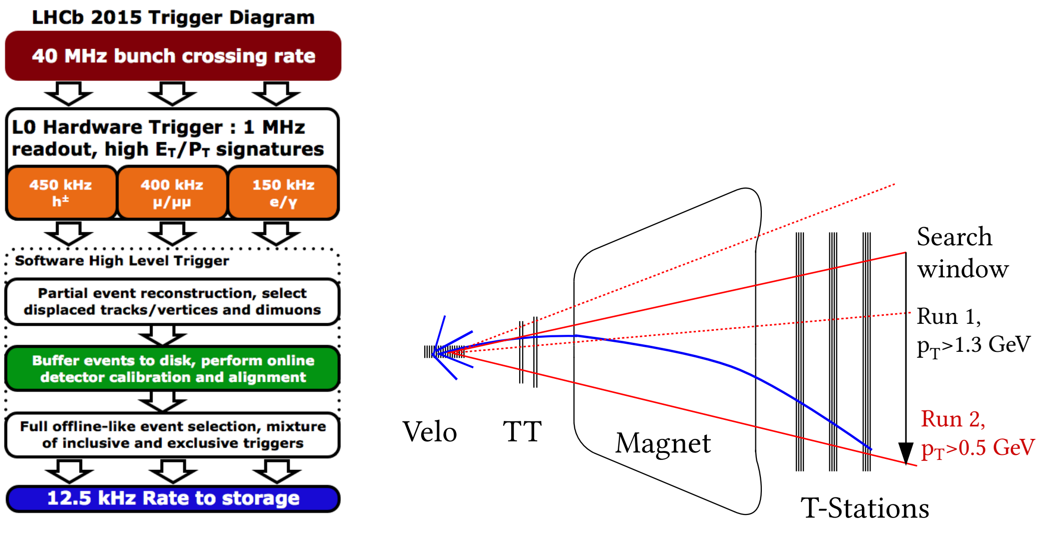
LHCb 2015 Trigger Diagram
40 MHz bunch crossing rate
L0 Hardware Trigger : 1 MHz readout, high E_T/P_T signatures
450 kHz $h^\pm$
400 kHz $\mu/\mu\mu$
150 kHz e/γ
Software High Level Trigger
Partial event reconstruction, select displaced tracks/vertices and dimuons
Buffer events to disk, perform online detector calibration and alignment
Full offline-like event selection, mixture of inclusive and exclusive triggers
12.5 kHz Rate to storage
Search window
Run 1, p_T>1.3 GeV
Run 2, p_T>0.5 GeV
Velo
TT
Magnet
T-Stations

Figure 3. Scheme of the trigger for Run II of LHCb (left). Scheme for the reconstruction of long tracks in Run I and Run II (right). Note that the p_T threshold could be lowered in Run II, allowing for a higher physics yield.

3 SIMD in LHCb

3.1 The need for speed

Even though the new sequence resulted in a reduction in execution time, a further decrease was needed. In order to achieve this, SIMD instructions were introduced. There were two main problems. Most of the code of the LHCb track reconstruction was written several years ago and was not adapted to make use of parallelization natively. Furthermore, a large part of the pattern recognition code consists of selecting the right clusters, tracks, etc., and therefore makes heavy use of branching. SIMD uses vector instructions, meaning that basic mathematical operations like addition and multiplication can be executed in parallel on more than one value. However, this only works if it is guaranteed that all values actually will be computed, and not discarded due to choosing the wrong branch. It is therefore best suited for those parts of the reconstruction code, where purely mathematical computations play a large role in the total time consumption.

SIMD instructions have seen a big evolution in the last 15 years. All CPUs used in the event-filter farm of LHCb can use at least the SSE2 instruction set, which allows processing two double or four float values in parallel. Accordingly, this was the architecture that was targeted.

3.2 Hough transform in forward tracking

In the forward algorithm, a VELO (or upstream) track, defining the position and the slopes, is matched to a single cluster in the T-stations. This completely defines all five parameters of the track. All clusters that belong to the same track should therefore accumulate in the same point when projected to a plane parallel to the tracking stations at a given point in z ("Hough plane"), assuming that the track model is correct and neglecting multiple scattering (see Figure 4). This accumulation can then be used to find valid track candidates. The projection of the cluster from its position in the detector plane to the Hough plane uses a third order polynomial, whose coefficients are derived in an iterative way. For each VELO track, all clusters have to be projected exactly once and they are independent of each other, which makes it an ideal case for SIMD instructions.

The overall reduction in time of using SIMD compared to processing the clusters sequentially is about 40%, which is close to the theoretical maximum of 50%, when using SSE2 and double values. The difference stems from the fact that the positions of the clusters are in a layout which needs to be made usable for SIMD first.

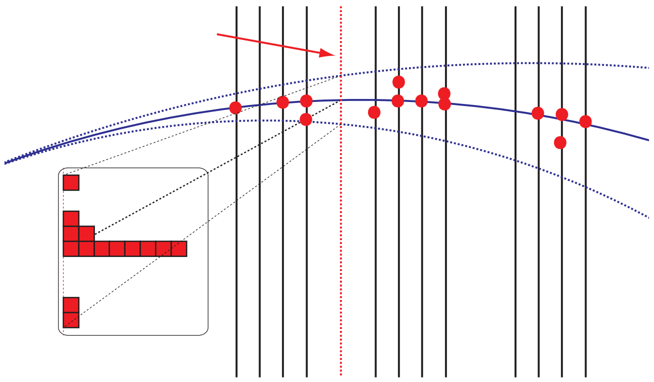

Figure 4. Illustration of the Hough transform. Clusters belonging to the same track (solid blue line) will accumulate around the same point in the Hough plane (red-dashed line) when being projected from their original position. Other clusters will be distributed randomly.

3.3 Computations in the Kalman Filter

All tracks found by the pattern recognition are subsequently fitted with a Kalman filter. The Kalman filter is very time consuming, making it the largest contributor time-wise in HLT1. A significant part of the time is spent in mathematical operations, where one important operation is the propagation of the covariance matrix of the state n to the state $n + 1$. This requires two multiplications of two 4x4 matrices F and C, such as $F \cdot C \cdot F^{T}$, where C is symmetric. However, a multiplication of two matrices can always be seen as the sum of the multiplications of a row with a single value (see Figure 5), which is ideal for using SIMD instructions. Reordering the multiplications such that they are vectorized reduced the time consumption by about a factor of 2. Using the AVX instruction set (which allows for the parallel processing of 4 double or 8 float values) would lead to a factor of five gain in speed, which is on average two floating point operations per CPU cycle.

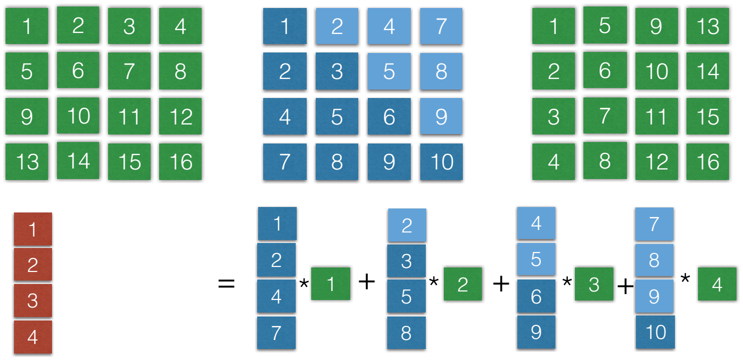

Figure 5. Illustration of the multiplication of three matrices, $F \cdot C \cdot F^{\mathrm{T}}$. The second row shows how the multiplication of the last two matrices can be decomposed in the sum of multiplications of a row-vector with a scalar value, which can be exploited with SIMD instructions.

4 Machine learning

Due to its long lever arm between the tracking stations before and after the magnet, a relatively large fraction of reconstructed tracks are “fake”, i.e. they do not correspond to a real charged particle having crossed the detector. In Run I, a cut on the χ^2/ndof of the tracks after the Kalman filter was applied. Later, the user of the data could select tracks with a low fake-probability by cutting on a quantity called “ghost probability”. This classifier was based on a neural net.

Approximately 22% of all reconstructed long tracks after the cut on χ^2/ndof were estimated to be fake in Run II. To further reduce this rate in the reconstruction, the idea was to use the ghost probability classifier directly in the final selection of tracks .

For Run II, the ghost probability is still based on a neural net, however it only uses variables as input which do not consume much computing power in the calculation. In total, 21 input variables are used. Most of them are taken from the result of the Kalman filter, like the overall χ^2/ndof, but also the χ^2/ndof of segments of the track, for example the TT – T-station segment. These segments might be more sensitive to detecting so called matching ghosts. They occur when a real VELO or upstream track and a real track in the T-stations are matched, although originating from different particles. The neural net consists of one hidden layer with 26 nodes. No gain in performance was seen by training a deep neural net. Likewise no gain was seen by using human assisted learning, i.e. forming new variables from the raw quantities as an input to the neural net.

To further speed up the calculation, the activation function of the neural net was chosen to be $1/\sqrt{1+x^2}$. This decreased the time consumption by a factor of 50 compared to using the hyperbolic tangent as activation function, which was the default in the Run I classifier.

All these improvements lead to an average time of the calculation of the ghost probability of 0.5ms per event; it therefore became possible to evaluate it in the high level trigger and to use it as a track-quality variable. The new scheme applies a combined cut on χ^2/ndof and ghost probability, which reduces the rate of fake tracks from 22% to 14%, without any loss of real tracks. An illustration of applying the ghost probability on tracks from $D^0 \to K\pi$ and $K_S \to \pi\pi$ decays can be seen in Figure 6.

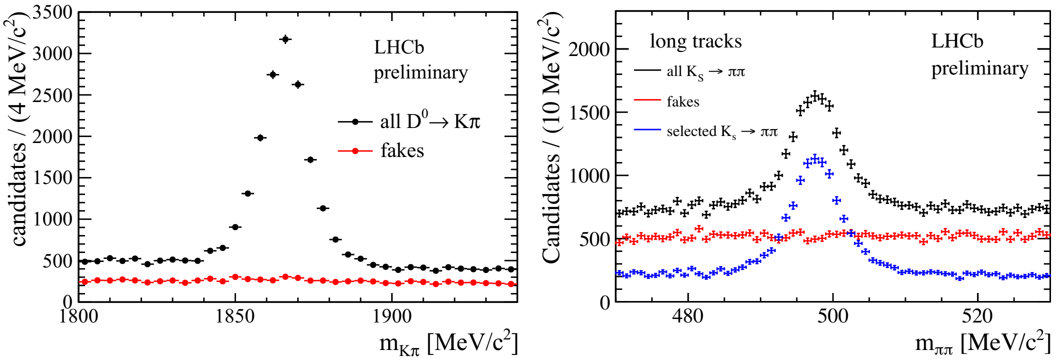

Figure 6. Performance of the ghost probability classifier for long tracks and $D^0 \to K\pi$ (left) and $K_S \to \pi\pi$ (right) decays. The rejected events are shown in red and show no peaking structure, meaning that no signal is lost with the cut on the ghost probability.

5 Total gain in timing

In addition to the presented points, many small-scale optimisations were performed in all the pattern recognition algorithms and in the Kalman filter, for example more efficient calculations or better use of the C++11 standard. The total speed-up, when comparing the reconstruction sequence in Run I and Run II, was a factor of 2, without any loss in performance. To achieve the same physics results without any modification of the code would have resulted in buying more machines for the HLT farm, whose total cost would have been several million Swiss francs.

6 Track reconstruction in the upgrade of LHCb

The LHCb detector will be upgraded in the long shutdown 2 of the LHC and restart taking data in 2020 at an instantaneous luminosity of $2 \cdot 10^{33}\,\text{cm}^{-2}\,\text{s}^{-1}$, which is about a factor of 5 more than the current instantaneous luminosity. At this luminosity, the rate of potentially interesting physics events would be too high for the L0 hardware trigger to handle. The idea is therefore to have only a software trigger which runs at the full bunch-crossing frequency. In order to achieve this goal, the tracking system needs to be replaced. The current VELO, a silicon strip detector, will be replaced by a pixel-based solution with a very high track reconstruction efficiency [11]. The TT-station before the magnet will be replaced by a silicon strip detector with a fine granularity [12]. The tracking stations behind the magnet will consist of 12 layers of a scintillating fiber tracker, which is read out by silicon photomultipliers [12].

The overall time available for track reconstruction is expected to be about 15 ms per event. This places strong constraints on all pattern recognition algorithms and the track fitter. The only way to achieve this goal is to exploit parallelisation, either using CPUs, or using other architectures, for example GPUs or Intel Xeon Phi. The main question is not only about the best raw performance, but mainly about the best performance for the amount of invested money.

6.1 Cellular automaton tracking

The search for standalone tracks in the T-stations is a highly parallelizable problem. For a given station (with its four layers in an *x*-*u*-*v*-*x* arrangement), for each cluster in a given layer, corresponding clusters have to be found in the other layers. One idea to perform this track reconstruction is to use a cellular automaton approach (see Ref. [13] for an example). First, tracklets between the two x layers in all three T-stations are reconstructed. Then stereo hits are added, leading to so-called “stubs”. These stubs now need to be connected between the three stations: Three-stations stubs are preferred over two-station stubs, as the latter are more likely to be fake tracks.

To test the efficiency of this approach (irrespective of the time consumption), a CPU implementation was written for the Run II detector. The track reconstruction efficiency of the cellular automaton approach is within a couple of percent of the nominal algorithm to reconstruct T tracks, where it has to be taken into account that the Run II algorithm has undergone extensive tuning over several years. The next step is now to port the algorithm to a GPU to test the performance not only for track reconstruction efficiency, but mainly for time consumption.

6.2 VELO tracking with GPUs

Another approach to gain experience with GPUs is to take an existing track reconstruction algorithm (in this case for the VELO standalone tracking), and to port it to a GPU, using the CUDA language [14]. This algorithm runs in “parasitic” mode in the monitoring farm of the HLT, meaning that it can be tested in real data taking conditions. While the efficiencies between the CPU and the GPU implementations are very similar, the GPU, as expected, shows an advantage when several events can be prepared in such a way that they can be processed in parallel, see Figure 7.

6.3 Structure of arrays

In order to optimally exploit SIMD instructions, the data needs to be provided in a “vectorization-friendly” way. At the moment, most classes in LHCb are arranged in an array-of-structures. For example, a cluster in a tracking detector is represented (in a simplified way) with a class “cluster” and holds three members, its coordinates x, y, z. A set of clusters therefore is arranged as an array of the cluster class. However, when using SIMD instructions, for example to calculate something with the x-coordinates only, the values are not sequential in memory. This prevents SIMD to process them simultaneously. The solution is to arrange the clusters in three arrays, each of them holding one coordinate only. This is less intuitive, but accessing the x-coordinates would mean accessing values which are next to each other in memory, greatly benefitting vectorization with SIMD.

Studies have started in LHCb that exploit the structure-of-array arrangement to speed up critical parts of the code.

7 Conclusion

For Run II, LHCb moved to a new trigger strategy with a real-time reconstruction, alignment and calibration. To fulfill the timing constraints, the track reconstruction was greatly sped up using SIMD instructions to increase the speed of the code and machine learning to efficiently remove fake tracks already in the reconstruction. Overall a gain of a factor of two in timing was obtained. The need for speed will continue in the upgrade of the LHCb detector, where a hardware trigger-less readout will necessitate the use of even faster algorithms, and therefore even more parallelized systems.

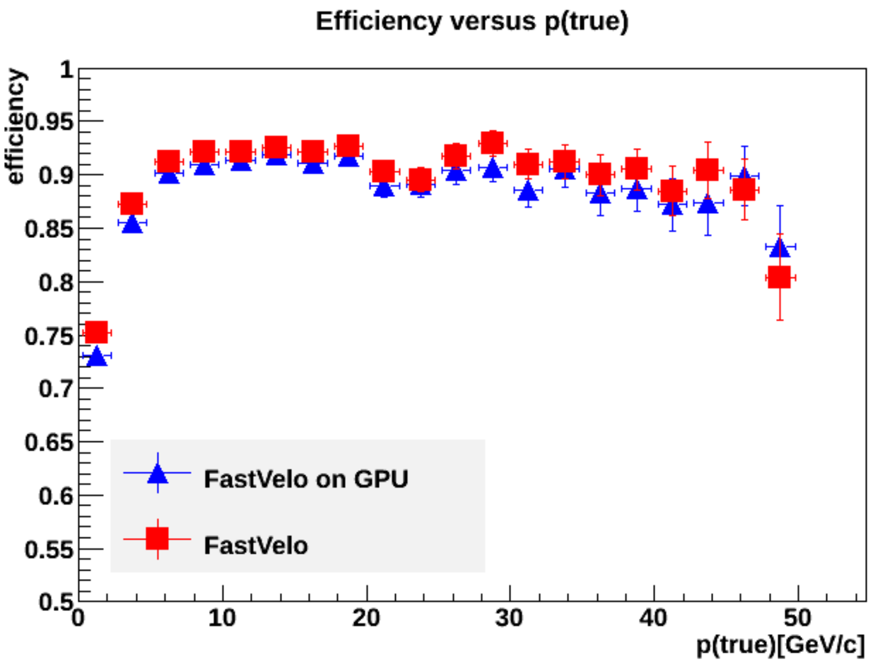

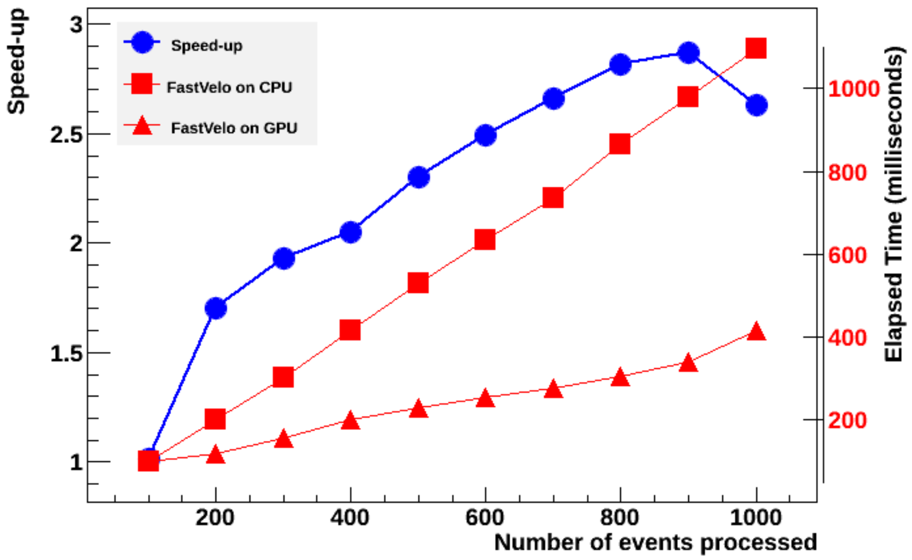

Figure 7. Left: Track reconstruction efficiency of the CPU based FastVELO algorithm (red) and its GPU implementation (blue) as a function of the momentum of the track. Right: Time consumption by the CPU (rectangle) and GPU (triangle) based FastVELO algorithm as a function of the number of processed events.

References

[1] Aaij, R. et al (2016), arXiv:1604.05596

[2] Alves, A. et al., JINST **3**, S08005 (2008)

[3] Aaij R. et al, Int. J. Mod. Phys. A **30**, 1530022 (2015), http://www.worldscientific.com/doi/pdf/10.1142/S0217751X15300227

[4] O. Callot, Tech. Rep. LHCb-PUB-2011-001. CERN-LHCb-PUB-2011-001, CERN, Geneva (2011), https://cds.cern.ch/record/1322644

[5] E.E. Bowen, B. Storaci, M. Tresch, Tech. Rep. LHCb-PUB-2015-024. CERN-LHCb-PUB-2015-024. LHCb-INT-2014-040, CERN, Geneva (2016), https://cds.cern.ch/record/2105078

[6] O. Callot, S. Hansmann-Menzemer, Tech. Rep. LHCb-2007-015. CERN-LHCb-2007-015, CERN, Geneva (2007), https://cds.cern.ch/record/1033584

[7] O. Callot, M. Schiller, Tech. Rep. LHCb-2008-042. CERN-LHCb-2008-042, CERN, Geneva (2008), https://cds.cern.ch/record/1119095

[8] M. Needham, J. Van Tilburg, Tech. Rep. LHCb-2007-020. CERN-LHCb-2007-020, CERN, Geneva (2007), https://cds.cern.ch/record/1020304

[9] M. Needham, Tech. Rep. LHCb-2007-129. CERN-LHCb-2007-129, CERN, Geneva (2007), https://cds.cern.ch/record/1060807

[10] O. Callot, Tech. Rep. LHCb-2007-026. CERN-LHCb-2007-026, CERN, Geneva (2007), https://cds.cern.ch/record/1025827

[11] LHCb Collaboration, Tech. Rep. CERN-LHCC-2013-021. LHCB-TDR-013, CERN, Geneva (2013), https://cds.cern.ch/record/1624070

[12] LHCb Collaboration, Tech. Rep. CERN-LHCC-2014-001. LHCB-TDR-015, CERN, Geneva (2014), https://cds.cern.ch/record/1647400

[13] I.S. Kulakov, S.A. Baginyan, V.V. Ivanov, P.I. Kisel, Phys. Part. Nuclei Letters **10**, 162 (2013)

[14] A. Badalov et al., Tech. Rep. LHCb-PUB-2014-034. CERN-LHCb-PUB-2014-034, CERN, Geneva (2014), https://cds.cern.ch/record/1698101